

## GEV GAMMA-RAY FLUX UPPER LIMITS FROM CLUSTERS OF GALAXIES

M. ACKERMANN<sup>2</sup>, M. AJELLO<sup>2</sup>, A. ALLAFORT<sup>2</sup>, L. BALDINI<sup>3</sup>, J. BALLET<sup>4</sup>, G. BARBIELLINI<sup>5,6</sup>, D. BASTIERI<sup>7,8</sup>, K. BECHTOL<sup>2,1</sup>, R. BELLAZZINI<sup>3</sup>, R. D. BLANDFORD<sup>2</sup>, P. BLASI<sup>9,1</sup>, E. D. BLOOM<sup>2</sup>, E. BONAMENTE<sup>10,11</sup>, A. W. BORGLAND<sup>2</sup>, A. BOUVIER<sup>2</sup>, T. J. BRANDT<sup>12,13</sup>, J. BREGEON<sup>3</sup>, M. BRIGIDA<sup>14,15</sup>, P. BRUEL<sup>16</sup>, R. BUEHLER<sup>2</sup>, S. BUSON<sup>7,8</sup>, G. A. CALIANDRO<sup>17</sup>, R. A. CAMERON<sup>2</sup>, P. A. CARAVEO<sup>18</sup>, S. CARRIGAN<sup>8</sup>, J. M. CASANDJIAN<sup>4</sup>, E. CAVAZZUTI<sup>19</sup>, C. CECCHEI<sup>10,11</sup>, Ö. ÇELIK<sup>20,21,22</sup>, E. CHARLES<sup>2</sup>, A. CHEKHTMAN<sup>23,24</sup>, C. C. CHEUNG<sup>23,25</sup>, J. CHIANG<sup>2</sup>, S. CIPRINI<sup>11</sup>, R. CLAUS<sup>2</sup>, J. COHEN-TANUGI<sup>26</sup>, S. COLAFRANCESCO<sup>19</sup>, L. R. COMINSKY<sup>27</sup>, J. CONRAD<sup>28,29,30</sup>, C. D. DERMER<sup>23</sup>, F. DE PALMA<sup>14,15</sup>, E. DO COUTO E SILVA<sup>2</sup>, P. S. DRELL<sup>2</sup>, R. DUBOIS<sup>2</sup>, D. DUMORA<sup>31,32</sup>, Y. EDMONDS<sup>2</sup>, C. FARNIER<sup>26</sup>, C. FAVUZZI<sup>14,15</sup>, M. FRAILIS<sup>33,34</sup>, Y. FUKAZAWA<sup>35</sup>, S. FUNK<sup>2,1</sup>, P. FUSCO<sup>14,15</sup>, F. GARGANO<sup>15</sup>, D. GASPARRINI<sup>19</sup>, N. GEHRELS<sup>20</sup>, S. GERMANI<sup>10,11</sup>, N. GIGLIETTO<sup>14,15</sup>, F. GIORDANO<sup>14,15</sup>, M. GIROLETTI<sup>36</sup>, T. GLANZMAN<sup>2</sup>, G. GODFREY<sup>2</sup>, I. A. GRENIER<sup>4</sup>, M.-H. GRONDIN<sup>31,32</sup>, S. GUIRIC<sup>37</sup>, D. HADASCH<sup>38</sup>, A. K. HARDING<sup>20</sup>, M. HAYASHIDA<sup>2</sup>, E. HAYS<sup>20</sup>, D. HORAN<sup>16</sup>, R. E. HUGHES<sup>13</sup>, T. E. JELTEMA<sup>39</sup>, G. JÓHANNesson<sup>2</sup>, A. S. JOHNSON<sup>2</sup>, T. J. JOHNSON<sup>20,40</sup>, W. N. JOHNSON<sup>23</sup>, T. KAMAE<sup>2</sup>, H. KATAGIRI<sup>35</sup>, J. KATAOKA<sup>41</sup>, M. KERR<sup>42</sup>, J. KNÖDLSEDER<sup>12</sup>, M. KUSS<sup>3</sup>, J. LANDE<sup>2</sup>, L. LATRONICO<sup>3</sup>, S.-H. LEE<sup>2</sup>, M. LEMOINE-GOUMAR<sup>31,32</sup>, F. LONGO<sup>5,6</sup>, F. LOPARCO<sup>14,15</sup>, B. LOTT<sup>31,32</sup>, M. N. LOVELLETTE<sup>23</sup>, P. LUBRANO<sup>10,11</sup>, G. M. MADEJSKI<sup>2</sup>, A. MAKEEV<sup>23,24</sup>, M. N. MAZZIOTTA<sup>15</sup>, P. F. MICHELSON<sup>2</sup>, W. MITTHUMSIRI<sup>2</sup>, T. MIZUNO<sup>35</sup>, A. A. MOISEEV<sup>21,40</sup>, C. MONTE<sup>14,15</sup>, M. E. MONZANI<sup>2</sup>, A. MORSELLI<sup>43</sup>, I. V. MOSKALENKO<sup>2</sup>, S. MURGIA<sup>2</sup>, M. NAUMANN-GODO<sup>4</sup>, P. L. NOLAN<sup>2</sup>, J. P. NORRIS<sup>44</sup>, E. NUSS<sup>26</sup>, T. OHSUGI<sup>45</sup>, N. OMODEI<sup>2</sup>, E. ORLANDO<sup>46</sup>, J. F. ORMES<sup>44</sup>, M. OZAKI<sup>47</sup>, D. PANQUE<sup>2</sup>, J. H. PANETTA<sup>2</sup>, M. PEPE<sup>10,11</sup>, M. PESCE-ROLLINS<sup>3</sup>, V. PETROSIAN<sup>2,1</sup>, C. PFROMMER<sup>48</sup>, F. PIRON<sup>26</sup>, T. A. PORTER<sup>2</sup>, S. PROFUMO<sup>39</sup>, S. RAINÒ<sup>14,15</sup>, R. RANDO<sup>7,8</sup>, M. RAZZANO<sup>3</sup>, A. REIMER<sup>49,2,1</sup>, O. REIMER<sup>49,2,1</sup>, T. REPOSEUR<sup>31,32</sup>, J. RIPKEN<sup>28,29</sup>, S. RITZ<sup>39</sup>, A. Y. RODRIGUEZ<sup>17</sup>, R. W. ROMANI<sup>2</sup>, M. ROTH<sup>42</sup>, H. F.-W. SADROZINSKI<sup>39</sup>, A. SANDER<sup>13</sup>, P. M. SAZ PARKINSON<sup>39</sup>, J. D. SCARLGE<sup>50</sup>, C. SGRO<sup>3</sup>, E. J. SISKIND<sup>51</sup>, P. D. SMITH<sup>13</sup>, G. SPANDRE<sup>3</sup>, P. SPINELLI<sup>14,15</sup>, J.-L. STARCK<sup>4</sup>, L. STAWARZ<sup>47,52</sup>, M. S. STRICKMAN<sup>23</sup>, A. W. STRONG<sup>46</sup>, D. J. SUSON<sup>53</sup>, H. TAJIMA<sup>2</sup>, H. TAKAHASHI<sup>45</sup>, T. TAKAHASHI<sup>47</sup>, T. TANAKA<sup>2</sup>, J. B. THAYER<sup>2</sup>, J. G. THAYER<sup>2</sup>, L. TIBALDO<sup>7,8,4,54</sup>, O. TIBOLLA<sup>55</sup>, D. F. TORRES<sup>17,38</sup>, G. TOSTI<sup>10,11</sup>, A. TRAMACERE<sup>2,56,57</sup>, Y. UCHIYAMA<sup>2</sup>, T. L. USHER<sup>2</sup>, J. VANDENBROUCKE<sup>2</sup>, V. VASILEIOU<sup>21,22</sup>, N. VILCHEZ<sup>12</sup>, V. VITALE<sup>43,58</sup>, A. P. WAITE<sup>2</sup>, P. WANG<sup>2</sup>, B. L. WINER<sup>13</sup>, K. S. WOOD<sup>23</sup>, Z. YANG<sup>28,29</sup>, T. YLINEN<sup>59,60,29</sup>, M. ZIEGLER<sup>39</sup>

*Draft version October 23, 2018*

## ABSTRACT

The detection of diffuse radio emission associated with clusters of galaxies indicates populations of relativistic leptons infusing the intracluster medium. Those electrons and positrons are either injected into and accelerated directly in the intracluster medium, or produced as secondary pairs by cosmic-ray ions scattering on ambient protons. Radiation mechanisms involving the energetic leptons together with decay of neutral pions produced by hadronic interactions have the potential to produce abundant GeV photons. Here, we report on the search for GeV emission from clusters of galaxies using data collected by the Large Area Telescope (LAT) on the *Fermi* Gamma-ray Space Telescope (*Fermi*) from August 2008 to February 2010. Thirty-three galaxy clusters have been selected according to their proximity and high mass, X-ray flux and temperature, and indications of non-thermal activity for this study. We report upper limits on the photon flux in the range 0.2–100 GeV towards a sample of observed clusters (typical values  $1\text{--}5 \times 10^{-9}$  ph cm $^{-2}$  s $^{-1}$ ) considering both point-like and spatially resolved models for the high-energy emission, and discuss how these results constrain the characteristics of energetic leptons and hadrons, and magnetic fields in the intracluster medium. The volume-averaged relativistic-hadron-to-thermal energy density ratio is found to be < 5–10 % in several clusters.

*Subject headings:* cosmic rays — galaxies: clusters: general — gamma rays: galaxies: clusters — radiation mechanisms: non-thermal

<sup>1</sup> Corresponding authors: K. Bechtol, bechtol@stanford.edu; P. Blasi, blasi@arcetri.astro.it; S. Funk, funk@slac.stanford.edu; V. Petrosian, vaher@stanford.edu; O. Reimer, olaf.reimer@uibk.ac.at

<sup>2</sup> W. W. Hansen Experimental Physics Laboratory, Kavli Institute for Particle Astrophysics and Cosmology, Department of Physics and SLAC National Accelerator Laboratory, Stanford University, Stanford, CA 94305, USA

<sup>3</sup> Istituto Nazionale di Fisica Nucleare, Sezione di Pisa, I-56127 Pisa, Italy

<sup>4</sup> Laboratoire AIM, CEA-IRFU/CNRS/Université Paris Diderot, Service d’Astrophysique, CEA Saclay, 91191 Gif sur Yvette, France

<sup>5</sup> Istituto Nazionale di Fisica Nucleare, Sezione di Trieste, I-34127 Trieste, Italy

<sup>6</sup> Dipartimento di Fisica, Università di Trieste, I-34127 Trieste, Italy

<sup>7</sup> Istituto Nazionale di Fisica Nucleare, Sezione di Padova, I-35131 Padova, Italy

<sup>8</sup> Dipartimento di Fisica “G. Galilei”, Università di Padova, I-35131 Padova, Italy

<sup>9</sup> Osservatorio Astrofisico di Arcetri, 50125 Firenze, Italy

<sup>10</sup> Istituto Nazionale di Fisica Nucleare, Sezione di Perugia, I-06123 Perugia, Italy

<sup>11</sup> Dipartimento di Fisica, Università degli Studi di Perugia, I-06123 Perugia, Italy

<sup>12</sup> Centre d’Étude Spatiale des Rayonnements, CNRS/UPS, BP 44346, F-30128 Toulouse Cedex 4, France

<sup>13</sup> Department of Physics, Center for Cosmology and Astro-Particle Physics, The Ohio State University, Columbus, OH 43210, USA

<sup>14</sup> Dipartimento di Fisica “M. Merlin” dell’Università e del Politecnico di Bari, I-70126 Bari, Italy

<sup>15</sup> Istituto Nazionale di Fisica Nucleare, Sezione di Bari, 70126 Bari, Italy

<sup>16</sup> Laboratoire Leprince-Ringuet, École polytechnique, CNRS/IN2P3, Palaiseau, France

<sup>17</sup> Institut de Ciencies de l’Espai (IEEC-CSIC), Campus UAB, 08193 Barcelona, Spain

<sup>18</sup> INAF-Istituto di Astrofisica Spaziale e Fisica Cosmica, I-20133 Milano, Italy

<sup>19</sup> Agenzia Spaziale Italiana (ASI) Science Data Center, I-00044 Frascati (Roma), Italy

<sup>20</sup> NASA Goddard Space Flight Center, Greenbelt, MD 20771, USA

<sup>21</sup> Center for Research and Exploration in Space Science and Technology

## 1. INTRODUCTION

Clusters of galaxies are the largest virialized structures in the Universe. In addition to a high concentration of galaxies, they contain ionized gas distributed in the intracluster medium (ICM) which emits thermal bremsstrahlung radiation in the soft X-ray (SXR; 2–10 keV) energy range. The dynamics of galaxies and thermal gas, together with gravitational lensing studies, indicate a dynamically dominant dark matter com-

(CRESST) and NASA Goddard Space Flight Center, Greenbelt, MD 20771, USA

<sup>22</sup> Department of Physics and Center for Space Sciences and Technology, University of Maryland Baltimore County, Baltimore, MD 21250, USA

<sup>23</sup> Space Science Division, Naval Research Laboratory, Washington, DC 20375, USA

<sup>24</sup> George Mason University, Fairfax, VA 22030, USA

<sup>25</sup> National Research Council Research Associate, National Academy of Sciences, Washington, DC 20001, USA

<sup>26</sup> Laboratoire de Physique Théorique et Astroparticules, Université Montpellier 2, CNRS/IN2P3, Montpellier, France

<sup>27</sup> Department of Physics and Astronomy, Sonoma State University, Rohnert Park, CA 94928-3609, USA

<sup>28</sup> Department of Physics, Stockholm University, AlbaNova, SE-106 91 Stockholm, Sweden

<sup>29</sup> The Oskar Klein Centre for Cosmoparticle Physics, AlbaNova, SE-106 91 Stockholm, Sweden

<sup>30</sup> Royal Swedish Academy of Sciences Research Fellow, funded by a grant from the K. A. Wallenberg Foundation

<sup>31</sup> CNRS/IN2P3, Centre d'Études Nucléaires Bordeaux Gradignan, UMR 5797, Gradignan, 33175, France

<sup>32</sup> Université de Bordeaux, Centre d'Études Nucléaires Bordeaux Gradignan, UMR 5797, Gradignan, 33175, France

<sup>33</sup> Dipartimento di Fisica, Università di Udine and Istituto Nazionale di Fisica Nucleare, Sezione di Trieste, Gruppo Collegato di Udine, I-33100 Udine, Italy

<sup>34</sup> Osservatorio Astronomico di Trieste, Istituto Nazionale di Astrofisica, I-34143 Trieste, Italy

<sup>35</sup> Department of Physical Sciences, Hiroshima University, Higashi-Hiroshima, Hiroshima 739-8526, Japan

<sup>36</sup> INAF Istituto di Radioastronomia, 40129 Bologna, Italy

<sup>37</sup> Center for Space Plasma and Aeronomy Research (CSPAR), University of Alabama in Huntsville, Huntsville, AL 35899, USA

<sup>38</sup> Institució Catalana de Recerca i Estudis Avançats (ICREA), Barcelona, Spain

<sup>39</sup> Santa Cruz Institute for Particle Physics, Department of Physics and Department of Astronomy and Astrophysics, University of California at Santa Cruz, Santa Cruz, CA 95064, USA

<sup>40</sup> Department of Physics and Department of Astronomy, University of Maryland, College Park, MD 20742, USA

<sup>41</sup> Research Institute for Science and Engineering, Waseda University, 3-4-1, Okubo, Shinjuku, Tokyo, 169-8555 Japan

<sup>42</sup> Department of Physics, University of Washington, Seattle, WA 98195-1560, USA

<sup>43</sup> Istituto Nazionale di Fisica Nucleare, Sezione di Roma "Tor Vergata", I-00133 Roma, Italy

<sup>44</sup> Department of Physics and Astronomy, University of Denver, Denver, CO 80208, USA

<sup>45</sup> Hiroshima Astrophysical Science Center, Hiroshima University, Higashi-Hiroshima, Hiroshima 739-8526, Japan

<sup>46</sup> Max-Planck Institut für extraterrestrische Physik, 85748 Garching, Germany

<sup>47</sup> Institute of Space and Astronautical Science, JAXA, 3-1-1 Yoshinodai, Sagamihara, Kanagawa 229-8510, Japan

<sup>48</sup> Canadian Institute for Theoretical Astrophysics, University of Toronto, Toronto, Ontario M5S 3H8, Canada

<sup>49</sup> Institut für Astro- und Teilchenphysik and Institut für Theoretische Physik, Leopold-Franzens-Universität Innsbruck, A-6020 Innsbruck, Austria

<sup>50</sup> Space Sciences Division, NASA Ames Research Center, Moffett Field, CA 94035-1000, USA

<sup>51</sup> NYCB Real-Time Computing Inc., Lattingtown, NY 11560-1025, USA

<sup>52</sup> Astronomical Observatory, Jagiellonian University, 30-244 Kraków, Poland

<sup>53</sup> Department of Chemistry and Physics, Purdue University Calumet, Hammond, IN 46323-2094, USA

ponent. Finally, many clusters show a ‘non-thermal’ (NT) emission (e.g. radio synchrotron) component signifying populations of relativistic leptons in combination with an appreciable magnetic field, and necessarily, turbulence and shocks permeating the ICM.

Galaxy clusters are also unique reservoirs of cosmic ray (CR) hadrons. Sparse thermal gas ( $n \sim 10^{-3} - 10^{-4} \text{ cm}^{-3}$ ) allows energetic ions to survive over cosmological timescales, leading in principle to a situation in which an appreciable fraction of the total cluster pressure is provided by accumulated CRs confined to the ICM by turbulence or chaotic magnetic fields (Völk et al. 1996; Berenzinsky et al. 1997). This scenario can be directly tested by gamma-ray telescopes (e.g. Enßlin et al. 1997; Colafrancesco & Blasi 1998; Berrington & Dermer 2004; Pfrommer & Enßlin 2004) because high-energy photons are expected to be produced either through inelastic proton-proton collisions and subsequent neutral-pion decay, or by processes involving energetic electron-positron pairs produced as secondaries of the hadronic interactions. CR leptons can also be injected by galaxies and active galactic nuclei and re-accelerated by turbulence and/or merger or accretion shocks in the ICM. In contrast to the CR ions, populations of relativistic leptons are expected to be shorter-lived (< Gyr; Petrosian 2001) and depend more upon recent merger events than on the full formation histories of their host clusters (Blasi et al. 2007 and references therein).

The presence of NT activity in the ICM of some clusters was first discovered as diffuse (relic or halo) radio emission by 1–10 GeV electrons (characterized by a power-law spectral distribution  $N_e(E) \propto E^{-p}$  with  $p > 3$ ) in the expected  $\mathcal{O}(\mu\text{G})$  magnetic fields. The radio emission appears to correlate with merger activity and SXR luminosity of the host cluster. Recently, excess fluxes beyond the expected thermal emission have been discovered in the extreme ultraviolet (EUV; 0.07–3 keV) and hard X-ray (HXR; 10–100 keV) ranges in several clusters by *EUVE*, *BeppoSAX*, *RXTE*, *Suzaku*, and *Integral* (Rephaeli et al. 2008). The extent and strength of these emissions has been disputed (e.g. analyses of *Swift*/BAT observations by Ajello et al. 2009, and *Suzaku* observations by Wik et al. 2009) and characterization of these radiations as thermal or NT remains controversial. However, the undisputed presence of radio-emitting leptons indicates that there will be gamma-ray emission by these leptons either by inverse Compton (IC) scattering of cosmic microwave background (CMB) and other soft (IR, optical, SXR) photons, or by NT bremsstrahlung scattering with background charged particles (e.g. Atoyan & Völk 2000; Reimer et al. 2004; Blasi et al. 2007). For details, see review by Petrosian et al. (2008) and references therein.

Unlike for the leptons, there is no direct observational evidence for CR ions in the ICM of any cluster. Previous observations by satellite-based “MeV/GeV” (Sreekumar et al.

<sup>54</sup> Partially supported by the International Doctorate on Astroparticle Physics (IDAPP) program

<sup>55</sup> Institut für Theoretische Physik und Astrophysik, Universität Würzburg, D-97074 Würzburg, Germany

<sup>56</sup> Consorzio Interuniversitario per la Fisica Spaziale (CIFS), I-10133 Torino, Italy

<sup>57</sup> INTEGRAL Science Data Centre, CH-1290 Versoix, Switzerland

<sup>58</sup> Dipartimento di Fisica, Università di Roma “Tor Vergata”, I-00133 Roma, Italy

<sup>59</sup> Department of Physics, Royal Institute of Technology (KTH), AlbaNova, SE-106 91 Stockholm, Sweden

<sup>60</sup> School of Pure and Applied Natural Sciences, University of Kalmar, SE-391 82 Kalmar, Sweden

1996; Reimer et al. 2003) and imaging air-Cherenkov “TeV” telescopes (Hattori & Nishijima 2005; Perkins et al. 2006; Perkins 2008; Galante et al. 2009; Aharonian et al. 2009a,b; Kiuchi et al. 2009; Aleksić et al. 2010), and shower particle detectors (Dingus et al. 2005) have provided gamma-ray flux upper limits which can constrain populations of hadronic CRs from GeV to multi-TeV energies.

An additional source of GeV gamma rays could be decay or annihilation of dark matter particles. Dark matter annihilation could also contribute to the pool of relativistic leptons. However, in view of the currently speculative nature of these mechanisms, conventional astrophysical processes should be fully understood before attributing observed gamma rays to dark matter annihilation. A dedicated analysis of *Fermi*-LAT observations of galaxy clusters in the context of specific dark matter models is presented separately (Abdo et al. 2010a).

In the next section, we describe the selection procedure for candidate clusters. §3 outlines our analysis of *Fermi*-LAT data and we present our results, consisting only of upper limits. We briefly discuss the constraints these observations place on the spectra and distribution of NT particles in the ICM in §4 and conclude with §5.

## 2. CANDIDATE SELECTION

The selection criteria of clusters with the greatest chance of detection at GeV gamma-ray energies are complicated, involving relativistic ions and electrons, magnetic fields, cluster merger history, and other properties of the ICM such as the thermal gas density and temperature. The gamma-ray flux from neutral-pion decay is expected to correlate with SXR flux since both emissions are related to the thermal gas density (Colafrancesco & Blasi 1998). Therefore, we began with the HIFLUCS flux-limited sample of the brightest X-ray clusters (Reiprich and Böhringer 2002) and selected clusters with the highest ratio of mass-to-distance-squared,  $M/d^2$ . To this sample, we added clusters with previously observed NT emission in other wavebands (e.g. diffuse radio features) as an indicator of relativistic lepton populations, and also clusters with exceptional X-ray luminosity and temperature such as the Bullet cluster ( $z = 0.296$ ; Clowe et al. 2004), MACSJ0717.5+3745 ( $z = 0.546$ ; Ebeling et al. 2007), and RJ1347.5-1145 ( $z = 0.451$ ; Schindler et al. 1995). The characteristics of thirty-three galaxy clusters selected for study in LAT data are provided in Table 1.

## 3. OBSERVATIONS, ANALYSIS, & RESULTS

The LAT is a pair-conversion telescope with a precision tracker and calorimeter, a segmented anti-coincidence detector (ACD) which covers the tracker array, and a programmable trigger and data acquisition system. The energy range of LAT sensitivity spans from 20 MeV to  $> 300$  GeV with an angular resolution per single event of approximately  $5.1^\circ$  at 100 MeV and narrowing to about  $0.14^\circ$  at 10 GeV.<sup>61</sup> Full details of the instrument, on-board and ground data processing, and other mission-oriented support are given in Atwood et al. (2009).

We searched for high-energy emission from thirty-three galaxy clusters using LAT data collected from the commencement of scientific operations in early-August 2008 to 4 February 2010. During this period, the LAT operated primarily in a

<sup>61</sup> Angular resolution is defined here as the 68% containment radius of the LAT point spread function averaged over the instrument acceptance and including photons which convert in either the thick or thin layers of the tracker array.

scanning mode (the ‘sky survey’ mode) that covered the full sky every two orbits (i.e.,  $\sim 3$  hrs). For operational reasons, the standard rocking angle (defined as the angle between the zenith and center of the LAT field of view) for survey mode was increased to  $50^\circ$  on 3 September 2009 and the data selection criteria for the present work have been adjusted accordingly relative to the 1FGL catalog analysis (Abdo et al. 2010b). We began by selecting all gamma rays of energy 0.2–100 GeV within a  $10^\circ$  radius around the direction of each galaxy cluster in our sample. Only events satisfying the standard low-background ‘diffuse’ class<sup>62</sup> selection criteria corresponding to the post-launch P6V3 instrument response functions are accepted into the following analysis. In order to reduce the effects of the so-called ‘albedo’ gamma rays (from interaction of CRs with the upper atmosphere), we remove photons arriving from zenith angles  $> 100^\circ$  and exclude time periods when the rocking angle exceeded  $52^\circ$ .

The data were prepared using the LAT Science Tools software package and analyzed in the context of diffuse gamma-ray emissions and discrete sources previously detected by the LAT.<sup>63</sup> Diffuse gamma-ray emission from the Milky Way is estimated using model templates from `gll_iem_v02.fit`. The isotropic diffuse component, attributed to both diffuse extragalactic gamma-ray emission and residual background of charged particles triggering the LAT, has been treated with `isotropic_iem_v02.txt`. In addition, all individual objects detected by the *Fermi*-LAT appearing in the 1FGL catalog (Abdo et al. 2010b) within a  $10^\circ$  radius of each candidate position are included in the sky model as separately-fit point sources with fixed position.

We created detection significance maps of the regions of the sky around each cluster using a maximum likelihood analysis tool (`sourcelike`). With the exception of the Perseus and Virgo clusters, no significant gamma-ray signal was detected by the LAT towards any galaxy cluster in our sample. The flux from the Perseus cluster is dominated by variable emission from NGC 1275 (probably related to the radio core 3C84; Abdo et al. 2009a) while the radio galaxy M87 appears to be the primary gamma-ray source of the Virgo cluster (Abdo et al. 2009b).

We determined flux upper limits for each cluster using the Neyman construction suitable for experiments with low signal counts in the presence of background. Confidence intervals were created using the Roe-Woodroffe (1999) modification to the unified approach proposed by Feldman and Cousins (1998). Within the full  $10^\circ$  radius region of interest centered on each cluster, we define an inner circular aperture for the purpose of comparing the observed counts to the number of photons expected from backgrounds alone. The radii of the inner apertures are optimized to maximize the signal-to-noise ratio given the particular background distributions and assumed extent of high-energy cluster emission. The radii of photon counting apertures are adjusted to maintain uniform signal containment over the 0.2–100 GeV energy range.

Several clusters in our sample are sufficiently extended to be potentially resolved by the LAT, depending on the (as yet unknown) spatial distributions of their gamma-ray emit-

<sup>62</sup> See [http://fermi.gsfc.nasa.gov/ssc/data/analysis/documentation/Cicerone/Cicerone\\_Data/LAT\\_DP.html](http://fermi.gsfc.nasa.gov/ssc/data/analysis/documentation/Cicerone/Cicerone_Data/LAT_DP.html).

<sup>63</sup> Information regarding the LAT Science Tools package, diffuse models, instrument response functions, and public data access is available from the *Fermi* Science Support Center (<http://fermi.gsfc.nasa.gov/ssc/>)

ting regions (see e.g. Pinzke & Pfrommer (2010) and Donnert et al. (2010) for gamma-ray surface intensity distributions predicted from numerical simulations). Since soft X-ray (bremsstrahlung) emissivity is proportional to the square of the thermal gas number density, then assuming that CRs reflect the thermal gas distribution, the expected surface brightness from hadronic gamma-ray emission should follow the X-ray emission. Therefore, we apply a King ( $\beta$ ) surface intensity profile with core radius  $r_c$ ,

$$\Sigma(r) = \Sigma(0) \left[ 1 + \left( \frac{r}{r_c} \right)^2 \right]^{-\beta+0.5}, \quad (1)$$

where X-ray profiles are available and can be sufficiently well-fit by this form (Chen et al. 2007; Matsushita et al. 2002 for the Virgo cluster). In addition, we have treated the Coma, Fornax, and Virgo clusters with two-dimensional Gaussian surface intensity models to assess the stability of the upper limits given the uncertain spatial distribution of high-energy cluster emission. Tables 2 and 3 provide 95% confidence-level flux upper limits in the energy range 0.2–100 GeV assuming unresolved (point-like) or spatially extended hypotheses, respectively. The gamma-ray flux upper limits presented here do not depend strongly on the particular surface intensity distributions of cluster emission.

Integral flux upper limits over a broad energy range depend partly upon the assumed spectrum of radiation because the LAT effective area increases between 0.2 and 1 GeV. Here, we assume a power-law spectrum of high-energy cluster emission with photon index  $\alpha_\gamma = 2$ . The degree to which upper limits computed with `sourcelike` depend upon the underlying spectrum of radiation can be estimated by rescaling the observation exposures according to the assumed source spectrum. For  $1.5 < \alpha_\gamma < 3.0$ , the relative change in photon flux upper limits in the energy ranges 0.2–100 GeV, 0.2–1 GeV, 1–10 GeV, and 10–100 GeV are 37%, 16%, 2%, and 1%, respectively, with the LAT being more sensitive to hard-spectrum sources. The 1–10 GeV energy band is typically the most sensitive in terms of average differential energy flux.

The flux upper limits to GeV emission from clusters of galaxies derived from LAT data are the most stringent to date. Upper limits set by EGRET (Reimer et al. 2003) and LAT observations are compared to recent model predictions in Figure 1. Although the LAT accumulated nearly uniform exposure over the full sky during the 18-month observation period, sensitivity to several candidates including the Ophiuchus and Perseus clusters is adversely affected by foreground emission from the Galactic plane and other bright gamma-ray sources.

#### 4. INTERPRETATION

We now use the flux upper limits provided by LAT observations to constrain NT populations of leptons ( $e^\pm$ ) and hadrons (protons and other ions) in the ICM. As described in §1, gamma rays can be produced from decay of  $\pi^0$ 's produced in proton-proton interactions between CR ions and ambient thermal gas. These collisions inevitably produce secondary  $e^\pm$  pairs which contribute to the population of energetic leptons in the ICM.

##### 4.1. Leptonic Emission Processes

Both primary and secondary electrons and positrons produce radio waves via synchrotron radiation in a magnetic field  $B \sim \mu\text{G}$  and gamma rays either by bremsstrahlung or

by IC scattering of ICM soft photons (energy density  $u_{\text{soft}}$ ). For a power-law electron spectrum,  $N(\gamma) = C\gamma^{-p}$ , the ratio of gamma-ray flux to radio flux (photon energy  $\epsilon_\gamma = h\nu$ ) from these processes is roughly  $\epsilon_\gamma F(\epsilon_\gamma)^{\text{brem}} / \epsilon_\gamma F(\epsilon_\gamma)^{\text{rad}} \propto n/B^{\frac{(p+1)}{2}}$  and  $\epsilon_\gamma F(\epsilon_\gamma)^{\text{IC}} / \epsilon_\gamma F(\epsilon_\gamma)^{\text{rad}} \propto u_{\text{ph}}/B^{\frac{(p+1)}{2}}$ . Thus, for clusters with measured radio flux and knowledge of particle and soft photon densities, upper limits on gamma-ray fluxes can constrain the volume-averaged value of the magnetic field. We use the Coma cluster to illustrate such an analysis. The radio spectrum can be fitted by a power law,  $\epsilon_\gamma F(\epsilon_\gamma)^{\text{rad}} \simeq 10^{-14} \left( \frac{\nu}{\text{GHz}} \right)^{-\frac{1}{4}} \text{erg cm}^{-2}\text{s}^{-1}$  for  $0.03 \text{ GHz} < \nu < 1 \text{ GHz}$ , requiring an electron distribution with index  $p \sim 3.5$  in the Lorentz factor range of  $2 \times 10^2 \left( \frac{B}{\mu\text{G}} \right)^{\frac{1}{2}} < \gamma < 5 \times 10^3 \left( \frac{B}{\mu\text{G}} \right)^{\frac{1}{2}}$ . Beyond this energy, the spectrum steepens either as a power law with the index higher by one (Rephaeli 1979) or with exponential cut-off (Schlickeiser et al. 1987), requiring corresponding steepening of the electron spectrum (Petrosian 2001).

For a power-law distribution, the IC flux is given by  $\epsilon_\gamma F(\epsilon_\gamma)^{\text{IC}} \propto \epsilon_\gamma^{\frac{(3-p)}{2}} u_{\text{soft}} \epsilon_{\text{soft}}^{\frac{(p-3)}{2}} A(p)$ , where  $A(p)$  depends only on the electron spectral index, thereby favoring IC scattering of CMB photons with the highest energy density of  $u_{\text{CMB}} \sim 0.26 \text{ eV cm}^{-3}$  and  $\epsilon_{\text{CMB}} \sim 0.001 \text{ eV}$ . However, for  $p > 3$ , the contribution of higher-energy seed photons with lower energy density becomes increasingly important. For example, optical photons of  $\epsilon_{\text{soft}} = 3 \text{ eV}$  and  $u_{\text{opt}} \sim 0.05 \text{ eV cm}^{-3}$  will have equal contribution to CMB for  $p = 4$ . Moreover, since the electron spectrum steepens for  $\gamma \geq 10^4$ , the contribution from CMB photons will come primarily from electrons above this energy so that (for both the power law or exponential cut-off) the main contribution in the GeV range will come from scattering of optical photons. Similarly, the gamma-ray flux due to IR photons will be a factor  $\gtrsim 100$  smaller.<sup>64</sup> A detailed calculation of the expected IC flux when combined with the upper limit set by *Fermi* implies a lower limit of  $\sim 0.15 \mu\text{G}$  on the volume-averaged magnetic field of the Coma cluster. Furthermore, the non-detection of diffuse gamma-ray emission towards any cluster during the first year of LAT observations disfavors lepton acceleration efficiencies in intracluster shocks  $\gtrsim 0.001$  (Gabici & Blasi 2004).

The bremsstrahlung flux of the above electrons will produce a steeper gamma-ray spectrum  $\epsilon_\gamma F(\epsilon_\gamma) \propto \epsilon_\gamma^{2-p}$  and will require slightly smaller magnetic field lower limit.

##### 4.2. Hadronic Emission Processes

For clusters with previously measured gas density ( $n$ ) and temperature ( $T$ ) profiles, gamma-ray flux upper limits can directly constrain the energy density stored in hadronic CR relative to the thermal energy density of the ambient ICM gas (e.g. Enßlin et al. 1997; Pfrommer & Enßlin 2004), expressed as

$$\left\langle \frac{\epsilon_{\text{CR}}}{\epsilon_{\text{TH}}} \right\rangle \equiv \frac{\int N_p(E) E dE}{\frac{3}{2} n k T}, \quad (2)$$

when averaging over the cluster volume. We assume a uniform power-law spectra of CR hadrons throughout the ICM,

<sup>64</sup> Klein-Nishina suppression in this case will steepen the gamma-ray spectrum above 20 GeV (electron energy  $> 10 \text{ GeV}$ ). IC scattering of more numerous SXR photons occurs in the Klein-Nishina regime for  $e^\pm$  of energy  $\gtrsim 100 \text{ MeV}$  which will suppress gamma-ray flux above 30 MeV.

$N_p(E) \propto E^{-\alpha_p}$ , and a spatial distribution which follows the thermal gas. Note that gamma-ray emissivity could be enhanced by a relative over-abundance of CR ions in central regions where thermal gas density is greatest. The CR-hadron-to-thermal energy density ratios for clusters with available X-ray data are presented in Table 3 for two possible CR spectral indices,  $\alpha_p$ . Using the Coma cluster as an example, we find  $\langle \epsilon_{CR}/\epsilon_{TH} \rangle < 0.05$  compared to the upper limit of  $< 0.1$ – $0.3$  obtained from analysis of EGRET observations (Reimer et al. 2004). The constraints presented here complement recent observations by the H.E.S.S. and MAGIC telescopes which have yielded upper limits to  $\langle \epsilon_{CR}/\epsilon_{TH} \rangle$  of  $< 0.2$  for the Coma cluster (Aharonian et al. 2009b) and  $< 0.05$  for the Perseus cluster (Aleksić et al. 2010; simplified model) considering populations of multi-TeV CR hadrons in the ICM. CR populations are unlikely to contribute significant pressure which would bias X-ray mass estimates of clusters.

The constraints on hadronic CR populations derived from LAT data are in agreement with limits placed by indirect methods (Brunetti et al. 2007; Churazov et al. 2008) and with the predictions of theoretical models and numerical simulations pointing out morphological and spectral difficulties (namely, observed radio spectra cut-offs) of explaining large-scale radio halos with purely secondary emission (e.g. Blasi et al. 2007 and references therein; Donnert et al. 2010). For the clusters examined thus far, multiwavelength evidence suggests that secondary electrons play a minor role in NT emission.

## 5. CONCLUSIONS

We have presented gamma-ray flux upper limits for thirty-three clusters of galaxies obtained from 18 months of *Fermi*-LAT observations which are robust with respect to uncertainty in both the spatial extent and spectrum of high-energy

cluster emission. These limits directly constrain the volume-averaged ratio of CR-hadron-to-thermal energy density content of several clusters in our sample to be  $< 5$ – $10\%$ . Using the Coma cluster as an example, we have also shown that for clusters with observed diffuse radio emission, gamma-ray flux upper limits can set lower limits on the magnetic field. Despite having not detected any galaxy cluster at GeV energies, continuing observations in the gamma-ray band offer the potential to decipher the nature of the NT activity, and the emission and acceleration mechanisms of energetic particles in the ICM.

The *Fermi* LAT Collaboration acknowledges generous ongoing support from a number of agencies and institutes that have supported both the development and the operation of the LAT as well as scientific data analysis. These include the National Aeronautics and Space Administration and the Department of Energy in the United States, the Commissariat à l’Energie Atomique and the Centre National de la Recherche Scientifique / Institut National de Physique Nucléaire et de Physique des Particules in France, the Agenzia Spaziale Italiana and the Istituto Nazionale di Fisica Nucleare in Italy, the Ministry of Education, Culture, Sports, Science and Technology (MEXT), High Energy Accelerator Research Organization (KEK) and Japan Aerospace Exploration Agency (JAXA) in Japan, and the K. A. Wallenberg Foundation, the Swedish Research Council and the Swedish National Space Board in Sweden.

Additional support for science analysis during the operations phase is gratefully acknowledged from the Istituto Nazionale di Astrofisica in Italy and the Centre National d’Études Spatiales in France.

## REFERENCES

- Abdo, A. A., et al. 2009a, ApJ, 699, 31
- Abdo, A. A., et al. 2009b, ApJ, 707, 55
- Abdo, A. A., et al. 2010a, accepted to JCAP [arXiv:astro-ph/1002.2239]
- Abdo, A. A., et al. 2010b, accepted to ApJSupp. Ser. [arXiv:astro-ph/1002.2280]
- Aharonian, F., et al. 2009a, A&A, 495, 27
- Aharonian, F., et al. 2009b, A&A, 502, 437
- Ajello, M., et al. 2009, ApJ, 690, 367
- Aleksić, J., et al. 2010, ApJ, 710, 634
- Atoyan, A. M., & Völk, H.J. 2000, ApJ, 535, 45
- Atwood, W. B., et al. 2009, ApJ, 697, 1071
- Berezinsky, V. S., Blasi, P., & Ptuskin, V. S. 1997, ApJ, 487, 529
- Berrington, R. C., & Dermer, C. D. 2003, ApJ, 594, 709
- Blasi, P., Gabici, S., & Brunetti, G. 2007, International Journal of Modern Physics A, 22, 681
- Brunetti, G. et al. 2007, ApJ, 670, L5
- Clowe, D., Gonzales, A., & Markevitch, M. 2004, ApJ, 604, 596
- Colafrancesco, S., & Blasi, P. 1998, APh, 9, 227
- Chen, Y., Reiprich, T. H., Böhringer, H., Ikebe, Y., & Zhang, Y.-Y. 2007, A&A, 466, 805
- Churazov, E., et al. 2008, MNRAS, 388, 1062
- Donnert, J., Dolag, K., Cassano, R., & Brunetti, G. 2010 [arXiv:astro-ph/1003.0336]
- Ebeling, H., et al. 2007, ApJ, 661, L33
- Edge, A. C., et al. 2003, MNRAS, 339, 913
- Enßlin, T. A., Bierman, P. L., Kronberg, P. P., & Wu, X. 1997, ApJ, 477, 560
- Feldman, G. J., & Cousins, R. D. 1998, Phys. Rev. D, 57, 3873
- Gabici, S., & Blasi, P. 2004, Astroparticle Phys., 20, 579
- Galante, N., et al. 2009, in 31st ICRC Conf. Proc. (Łódź, Poland) [arXiv/astro-ph/0907.5000]
- Giovannini, G., Tordi, M., & Feretti, L. 1999, NewA, 4, 141
- Giovannini, G., & Feretti, L. 2000, NewA, 5, 335
- Govoni, F., et al. 2009, 499, 371
- Hattori, T., & Nishijima, K. 2005, Astrophysics and Space Science, 297, 327
- Kempner, J. C., & Sarazin, C. L. 2001, ApJ, 548, 639
- Kiuchi, R., et al. 2009, ApJ, 704, 240
- Liang, H., Hunstead, R. W., Birkhshaw, M., & Andreani, P. 2000, ApJ, 544, 686
- Matsushita, K., Belsole, E., Finoguenov, A., & Böhringer, H. 2002, A&A, 386, 77
- Pinzke, A., & Pfrommer, C. 2010, submitted to MNRAS [arXiv/astro-ph/1001.5023]
- Perkins, J. S. et al. 2006, ApJ, 644, 148
- Perkins, J. S. 2008, AIPC, 1085, 569
- Petrosian, V. 2001, ApJ, 557, 560
- Petrosian, V., Bykov, A., & Repaeli, Y. 2008, Space Sci. Rev., 134, 191
- Pfrommer, C., & Enßlin, T. A. 2004, A&A, 413, 17
- Reiprich, T. H., & Böhringer, H. 2002, ApJ, 567, 716
- Reimer, A., Reimer, O., Schlickeiser, R., Iyudin, A. 2004, A&A, 424, 773
- Reimer, O., et al. 2003, ApJ, 588, 155
- Rephaeli, Y. 1979, ApJ, 227, 364
- Rephaeli, Y., Nevalainen, J., Ohashi, T., & Bykov, A. M. 2008, Space Sci. Rev., 134, 71
- Roe, B. P., & Woodroffe, M. B. 1999, Phys. Rev. D, 60, 053009
- Schindler, S., et al. 1995, A&A, 299, L9
- Schlickeiser, R., Sievers, A., & Thiemann, H. 1987, A&A, 182, 21
- Sreekumar, P., et al. 1996, ApJ, 464, 628
- Völk, H. J., Aharonian, F. A., & Breitschwerdt, D. 1996, Space Sci. Rev., 75, 279
- Wik, D. R., et al. 2009, ApJ, 696, 1700

TABLE 1  
SUMMARY OF THE THIRTY-THREE GALAXY CLUSTER CANDIDATES

| Cluster                      | <i>l</i><br>(deg) | <i>b</i><br>(deg) | <i>z</i> | $\theta_{500}$<br>(deg) | $\theta_{core}$<br>(deg) | $M_{500}/d^2$<br>( $10^9 M_\odot/Mpc^2$ ) | Diffuse radio      | $L_X$ (0.1-2.4 keV)<br>( $10^{44} \text{ erg s}^{-1}$ ) | $T_X$<br>(keV) |
|------------------------------|-------------------|-------------------|----------|-------------------------|--------------------------|---|--------------------|---|----------------|
| <b>X-ray flux selection</b>  |                   |                   |          |                         |                          |   |                    |   |                |
| 3C129                        | 160.43            | 0.14              | 0.0223   | 0.67                    | 0.14                     | 29.1                                      | ...                | 2.27  | 5.57           |
| A0754                        | 239.25            | 24.75             | 0.0528   | 0.40                    | 0.05                     | 12.8                                      | ...                | 3.97  | 9.00           |
| A1367                        | 234.80            | 73.03             | 0.0216   | 0.77                    | 0.18                     | 42.7                                      | ...                | 1.20  | 3.55           |
| A2199                        | 62.94             | 43.69             | 0.0302   | 0.46                    | 0.05                     | 12.5                                      | ...                | 4.20  | 4.28           |
| A2256                        | 111.10            | 31.74             | 0.0601   | 0.33                    | 0.10                     | 8.5                                       | Halo, Relic (1, 2) | 9.24  | 6.83           |
| A2319                        | 75.67             | 13.58             | 0.0564   | 0.37                    | 0.05                     | 10.9                                      | Halo (1, 2)        | 16.37   | 8.84           |
| A3376                        | 246.52            | -26.29            | 0.0455   | 0.36                    | 0.17                     | 8.5                                       | ...                | 2.16  | 4.43           |
| A3571                        | 316.32            | 28.55             | 0.0397   | 0.45                    | 0.05                     | 14.5                                      | ...                | 8.08  | 6.80           |
| Antlia (S636)                | 272.94            | 19.19             | 0.0116   | 0.85                    | 0.29                     | 31.6                                      | ...                | 0.38  | 2.06           |
| AWM7                         | 146.35            | -15.62            | 0.0172   | 0.85                    | 0.10                     | 45.0                                      | ...                | 2.10  | 3.70           |
| Centaurus (A3526)            | 302.41            | 21.56             | 0.0499   | 1.24                    | 0.04                     | 87.9                                      | ...                | 1.19  | 3.69           |
| Coma (A1656)                 | 58.09             | 87.96             | 0.0232   | 0.80                    | 0.15                     | 49.6                                      | Halo, Relic (1)    | 8.09  | 8.07           |
| Fornax (S373)                | 236.72            | -53.64            | 0.0046   | 2.01                    | 0.36                     | 168.1                                     | ...                | 0.08  | 1.56           |
| Hydra (A1060)                | 269.63            | 26.51             | 0.0114   | 1.02                    | 0.08                     | 52.5                                      | ...                | 0.56  | 3.15           |
| M49                          | 286.92            | 70.17             | 0.0044   | 1.68                    | 0.02                     | 95.5                                      | ...                | 0.02  | 1.33           |
| NGC4636                      | 297.75            | 65.47             | 0.0037   | 1.27                    | 0.02                     | 36.3                                      | ...                | 0.02  | 0.66           |
| NGC5044                      | 311.23            | 46.10             | 0.0090   | 0.74                    | 0.01                     | 16.6                                      | ...                | 0.18  | 1.22           |
| NGC5813                      | 359.18            | 49.85             | 0.0064   | 1.00                    | 0.04                     | 28.9                                      | ...                | 0.02  | 0.76           |
| NGC5846                      | 0.43              | 48.80             | 0.0061   | 0.78                    | 0.01                     | 13.3                                      | ...                | 0.01  | 0.64           |
| Norma (A3627)                | 325.33            | -7.26             | 0.0163   | 0.89                    | 0.18                     | 50.2                                      | ...                | 3.59  | 5.62           |
| Ophiuchus                    | 0.56              | 9.27              | 0.0280   | 0.10                    | 0.10                     | 131.6                                     | Halo (3)           | 12.14   | 10.25          |
| Perseus (A0426)              | 150.58            | -13.26            | 0.0183   | 0.85                    | 0.03                     | 49.0                                      | ...                | 16.39   | 6.42           |
| Triangulum                   | 324.48            | -11.63            | 0.0510   | 0.42                    | 0.06                     | 14.7                                      | ...                | 12.43   | 9.06           |
| <b>Non-thermal selection</b> |                   |                   |          |                         |                          |   |                    |   |                |
| A0085                        | 115.05            | -72.06            | 0.0556   | 0.31                    | 0.02                     | ...                                       | Relic (1, 4)       | 9.67  | 6.51           |
| A1914                        | 67.20             | 67.46             | 0.1712   | 0.13                    | 0.02                     | ...                                       | Halo (1, 2)        | 17.04   | 8.41           |
| A2029                        | 6.51              | 50.55             | 0.0767   | 0.25                    | 0.01                     | ...                                       | Halo (3)           | 17.07   | 7.93           |
| A2142                        | 44.21             | 48.70             | 0.0899   | 0.24                    | 0.02                     | ...                                       | Halo (4)           | 21.05   | 8.46           |
| A2163                        | 6.75              | 30.52             | 0.2010   | 0.12                    | 0.03                     | ...                                       | Halo (1)           | 32.16   | 10.55          |
| A2744                        | 8.90              | -81.24            | 0.3080   | ...                     | ...                      | ...                                       | Halo (1)           | ...   | ...            |
| Bullet (1E 0657-56) (a)      | 266.03            | -21.25            | 0.296    | ...                     | ...                      | ...                                       | Halo (5)           | ...   | 14             |
| MACSJ0717.5+3745 (b)         | 61.89             | 34.02             | 0.546    | ...                     | ...                      | ...                                       | Relic (6)          | 24.6  | 11.6           |
| <b>Other selection</b>       |                   |                   |          |                         |                          |   |                    |   |                |
| RXJ1347.5-1145 (c)           | 324.04            | 48.80             | 0.451    | ...                     | ...                      | ...                                       | ...                | 62.0  | ...            |
| Virgo (M87 sub-clump) (d)    | 283.78            | 74.49             | 0.0036   | ...                     | 0.05                     | ...                                       | ...                | ...   | ...            |

X-ray measurements from Chen et al. 2007 unless stated otherwise. Other X-ray references: (a) Clowe et al. 2004; (b) Ebeling et al. 2007; (c) Schindler et al. 1995; (d) Matsushita et al. 2002. Radio references: (1) Giovannini et al. 1999 and references therein; (2) Kempner & Sarazin 2001; (3) Govoni et al. 2009; (4) Giovannini & Feretti 2000; (5) Liang et al. 2000; (6) Edge et al. 2003. A  $\Lambda$ CDM cosmology with Hubble constant  $H_0 = 50 \text{ km s}^{-1} \text{ Mpc}^{-1}$  is used for comparison to X-ray data sets.

TABLE 2

95% CONFIDENCE-LEVEL GAMMA-RAY FLUX UPPER LIMITS FROM CLUSTERS OF GALAXIES: EMISSION UNRESOLVED BY THE LAT (POINT SOURCE)

| Cluster    | $f_{src}$ | $N$<br>0.2-100 | $\langle \epsilon_\gamma F(\epsilon_\gamma) \rangle$<br>0.2-100 | $\langle \epsilon_\gamma F(\epsilon_\gamma) \rangle$<br>0.2-1 | $\langle \epsilon_\gamma F(\epsilon_\gamma) \rangle$<br>1-10 | $\langle \epsilon_\gamma F(\epsilon_\gamma) \rangle$<br>10-100 |
|------------|-----------|----------------|---|---|--|--|
| 3C129      | 0.54      | 3.44           | 1.10  | 2.04  | 1.06   | 1.84   |
| A0754      | 0.51      | 3.42           | 1.10  | 1.54  | 0.72   | 2.15   |
| A1367      | 0.49      | 1.65           | 0.53  | 0.97  | 0.93   | 2.13   |
| A1689      | 0.50      | 4.96           | 1.59  | 2.14  | 0.66   | 2.16   |
| A1914      | 0.54      | 1.19           | 0.38  | 0.72  | 0.57   | 1.86   |
| A2029      | 0.49      | 3.28           | 1.05  | 1.75  | 1.20   | 2.16   |
| A2142      | 0.52      | 2.82           | 0.90  | 1.59  | 0.45   | 1.95   |
| A2163      | 0.54      | 5.51           | 1.77  | 2.25  | 2.04   | 1.99   |
| A2199      | 0.52      | 1.12           | 0.72  | ...   | 0.56   | 1.91   |
| A2256      | 0.48      | 1.96           | 0.63  | 0.85  | 0.70   | 1.75   |
| A2319      | 0.51      | 0.75           | 0.24  | 0.42  | 0.54   | 1.91   |
| A2744      | 0.54      | 2.49           | 0.80  | 1.39  | 0.40   | 2.01   |
| A3266      | 0.56      | 9.23           | 2.96  | 4.08  | 0.61   | 1.85   |
| A3376      | 0.57      | 9.93           | 3.18  | 5.18  | 1.18   | 1.89   |
| A3571      | 0.51      | 2.80           | 0.90  | 1.66  | 0.84   | 2.13   |
| A3888      | 0.44      | 2.41           | 0.77  | 1.36  | 0.72   | 2.47   |
| A85        | 0.46      | 2.13           | 0.68  | 1.12  | 0.53   | 2.35   |
| AWM7       | 0.55      | 3.84           | 1.23  | 1.96  | 0.82   | 1.82   |
| Antilia    | 0.51      | 4.05           | 1.30  | 2.45  | 0.49   | 2.13   |
| Bullet     | 0.47      | 2.75           | 0.88  | 1.46  | 0.78   | 2.24   |
| Centaurus  | 0.51      | 8.01           | 2.57  | 4.12  | 1.35   | 2.13   |
| Coma       | 0.51      | 4.58           | 1.47  | 1.98  | 0.77   | 2.01   |
| Fornax     | 0.54      | 5.06           | 1.62  | 3.13  | 0.29   | 2.00   |
| Hydra      | 0.60      | 2.21           | 0.71  | 0.96  | 0.73   | 1.81   |
| M49        | 0.52      | 2.02           | 0.65  | 1.13  | 0.40   | 2.05   |
| MACSJ0717  | 0.54      | 6.63           | 2.13  | 2.89  | 1.11   | 1.84   |
| NGC4636    | 0.47      | 2.96           | 0.95  | 1.81  | 0.45   | 2.29   |
| NGC5044    | 0.50      | 1.90           | 0.61  | 0.88  | 0.62   | 2.18   |
| NGC5813    | 0.52      | 10.51          | 3.37  | 4.22  | 1.06   | 2.06   |
| NGC5846    | 0.55      | 13.02          | 4.18  | 5.38  | 0.69   | 1.94   |
| Norma      | 0.47      | 1.31           | 0.42  | 0.82  | 0.77   | 3.47   |
| Ophiuchus  | 0.54      | 26.22          | 8.41  | 13.32   | 2.11   | 2.00   |
| Perseus    | 0.68      | 89.19          | 28.60   | 30.34   | 28.76  | 12.92  |
| RXJ1347    | 0.55      | 2.57           | 0.82  | 1.17  | 0.49   | 1.98   |
| Triangulum | 0.54      | 2.68           | 0.86  | 0.90  | 0.97   | 1.93   |
| Virgo      | 0.62      | 14.13          | 4.53  | 4.97  | 3.89   | 2.67   |

$f_{src}$  is the estimated signal fraction captured within the photon counting aperture.  $N$  and  $\langle \epsilon_\gamma F(\epsilon_\gamma) \rangle$  correspond to the integral photon flux ( $10^{-9} \text{ ph cm}^{-2} \text{ s}^{-1}$ ) and average differential energy flux ( $10^{-12} \text{ erg cm}^{-2} \text{ s}^{-1}$ ), respectively, within the energy range provided (GeV) assuming a power-law spectrum of gamma-ray emission with photon index  $\alpha_\gamma=2$ . Only photons of energy 0.4-100 GeV were considered in the analysis of A2199 in order to reduce background from nearby bright sources.

TABLE 3  
95% CONFIDENCE-LEVEL GAMMA-RAY FLUX UPPER LIMITS FROM CLUSTERS OF GALAXIES: SPATIALLY EXTENDED EMISSION MODELS

| Cluster    | Spatial model ( $R_{68}$ )<br>(deg) | $f_{src}$ | $N$   | $\langle \epsilon_\gamma F(\epsilon_\gamma) \rangle$<br>0.2-100 | $\langle \epsilon_\gamma F(\epsilon_\gamma) \rangle$<br>0.2-100 | $\langle \epsilon_\gamma F(\epsilon_\gamma) \rangle$<br>0.2-1 | $\langle \epsilon_\gamma F(\epsilon_\gamma) \rangle$<br>1-10 | $\langle \epsilon_\gamma F(\epsilon_\gamma) \rangle$<br>10-100 | $\langle \epsilon_{CR}/\epsilon_{Th} \rangle$<br>$\alpha_p=2.1$ | $\langle \epsilon_{CR}/\epsilon_{Th} \rangle$<br>$\alpha_p=2.4$ |
|------------|-------------------------------------|-----------|-------|---|---|---|--|--|---|---|
| 3C129      | King                                | 0.56      | 3.93  | 1.26  | 1.84  | 1.01 <sup>†</sup>   | 2.61   | 0.16   | 0.12  |   |
| A0085      | King                                | 0.46      | 2.23  | 0.71  | 1.17  | 0.53 <sup>†</sup>   | 2.35   | 0.06   | 0.04  |   |
| A0754      | King                                | 0.54      | 3.31  | 1.06  | 1.65  | 1.06 <sup>†</sup>   | 2.03   | 0.35   | 0.27  |   |
| A1367      | King                                | 0.48      | 1.83  | 0.59  | 1.03 <sup>†</sup>   | 1.09  | 2.18   | 0.26   | 0.16  |   |
| A1914      | King                                | 0.54      | 1.18  | 0.38 <sup>†</sup>   | 0.72  | 0.57  | 1.86   | 0.38   | 0.24  |   |
| A2029      | King                                | 0.49      | 3.18  | 1.02  | 1.72  | 1.19 <sup>†</sup>   | 2.16   | 0.11   | 0.09  |   |
| A2142      | King                                | 0.52      | 2.75  | 0.88  | 1.59  | 0.49 <sup>†</sup>   | 1.95   | 0.07   | 0.05  |   |
| A2163      | King                                | 0.54      | 5.50  | 1.76 <sup>†</sup>   | 2.32  | 2.17  | 1.99 <sup>†</sup>  | 0.81   | 0.61  |   |
| A2199      | King                                | 0.51      | 1.18  | 0.76  | ...   | 0.54 <sup>†</sup>   | 1.95   | 0.14   | 0.11  |   |
| A2256      | King                                | 0.47      | 1.83  | 0.59  | 0.81  | 0.66 <sup>†</sup>   | 1.79   | 0.16   | 0.12  |   |
| A2319      | King                                | 0.54      | 0.73  | 0.23 <sup>†</sup>   | 0.54  | 0.58  | 2.82   | 0.03   | 0.02  |   |
| A3376      | King                                | 0.57      | 9.69  | 3.11  | 5.18  | 1.08 <sup>†</sup>   | 1.89   | 1.21   | 0.95  |   |
| A3571      | King                                | 0.50      | 3.26  | 1.04  | 1.85  | 0.89 <sup>†</sup>   | 2.17   | 0.05   | 0.04  |   |
| Antlia     | King                                | 0.52      | 4.84  | 1.55  | 2.86  | 0.66 <sup>†</sup>   | 2.09   | 1.52   | 1.19  |   |
| AWM7       | King                                | 0.55      | 3.95  | 1.27  | 1.92  | 0.97 <sup>†</sup>   | 1.82   | 0.10   | 0.08  |   |
| Centaurus  | King                                | 0.51      | 8.15  | 2.61  | 3.90  | 1.33 <sup>†</sup>   | 2.13   | 0.09   | 0.07  |   |
| Coma       | Gauss (0.2)                         | 0.53      | 4.84  | 1.55  | 2.28  | 0.76  | 3.03   | ...  | ...   |   |
| Coma       | Gauss (0.4)                         | 0.52      | 4.86  | 1.56  | 2.36  | 0.82  | 3.08   | ...  | ...   |   |
| Coma       | Gauss (0.6)                         | 0.58      | 5.12  | 1.64  | 2.38  | 0.82  | 4.97   | ...  | ...   |   |
| Coma       | Gauss (0.8)                         | 0.56      | 4.93  | 1.58  | 2.73  | 0.74  | 4.88   | ...  | ...   |   |
| Coma       | King                                | 0.55      | 5.14  | 1.65  | 2.18  | 1.11 <sup>†</sup>   | 2.92   | 0.05   | 0.04  |   |
| Fornax     | Gauss (0.2)                         | 0.51      | 4.77  | 1.53  | 2.61  | 0.31  | 2.12   | ...  | ...   |   |
| Fornax     | Gauss (0.4)                         | 0.62      | 5.40  | 1.73  | 2.73  | 0.39  | 2.72   | ...  | ...   |   |
| Fornax     | Gauss (0.6)                         | 0.59      | 5.73  | 1.84  | 3.02  | 0.43  | 2.68   | ...  | ...   |   |
| Fornax     | Gauss (0.8)                         | 0.62      | 5.39  | 1.73  | 2.61  | 0.89  | 2.28   | ...  | ...   |   |
| Fornax     | Gauss (1.0)                         | 0.60      | 5.03  | 1.61  | 2.87  | 0.90  | 2.30   | ...  | ...   |   |
| Fornax     | King                                | 0.60      | 5.64  | 1.81  | 2.80  | 0.40 <sup>†</sup>   | 2.81   | 0.75   | 0.59  |   |
| Hydra      | King                                | 0.60      | 2.24  | 0.72 <sup>†</sup>   | 0.94  | 0.85 <sup>†</sup>   | 2.83   | 0.28   | 0.21  |   |
| M49        | King                                | 0.52      | 2.08  | 0.67  | 1.14  | 0.39 <sup>†</sup>   | 2.05   | 5.09   | 3.98  |   |
| NGC4636    | King                                | 0.46      | 2.67  | 0.86  | 1.28  | 0.42 <sup>†</sup>   | 2.34   | 3.89   | 3.04  |   |
| NGC5044    | King                                | 0.50      | 1.87  | 0.60  | 0.81  | 0.62 <sup>†</sup>   | 2.18   | 1.58   | 1.24  |   |
| NGC5813    | King                                | 0.52      | 10.57 | 3.39  | 4.25  | 0.99 <sup>†</sup>   | 2.06   | 25.59  | 20.03   |   |
| NGC5846    | King                                | 0.55      | 13.01 | 4.17  | 5.38  | 0.69 <sup>†</sup>   | 1.94   | 13.82  | 10.82   |   |
| Norma      | King                                | 0.54      | 1.21  | 0.39 <sup>†</sup>   | 0.94  | 0.83  | 3.84   | 0.03   | 0.02  |   |
| Ophiuchus  | King                                | 0.54      | 26.22 | 8.41  | 14.18   | 2.02 <sup>†</sup>   | 1.95   | 0.05   | 0.04  |   |
| Perseus    | King                                | 0.70      | 87.36 | 28.01   | 28.11   | 29.02 <sup>†</sup>  | 17.95 <sup>†</sup>   | 0.27   | 0.32  |   |
| Triangulum | King                                | 0.54      | 2.39  | 0.77 <sup>†</sup>   | 0.91  | 1.03 <sup>†</sup>   | 1.93   | 0.07   | 0.05  |   |
| Virgo      | Gauss (0.2)                         | 0.62      | 14.49 | 4.65  | 4.93  | 4.13  | 4.35   | ...  | ...   |   |
| Virgo      | Gauss (0.4)                         | 0.61      | 15.27 | 4.90  | 5.26  | 4.65  | 5.13   | ...  | ...   |   |
| Virgo      | Gauss (0.6)                         | 0.64      | 14.97 | 4.80  | 5.62  | 4.72  | 4.48   | ...  | ...   |   |
| Virgo      | Gauss (0.8)                         | 0.64      | 15.76 | 5.05  | 5.62  | 4.72  | 4.48   | ...  | ...   |   |
| Virgo      | Gauss (1.0)                         | 0.66      | 16.01 | 5.13  | 5.71  | 4.59  | 4.35   | ...  | ...   |   |
| Virgo      | Gauss (1.2)                         | 0.64      | 17.03 | 5.46  | 5.62  | 4.72  | 4.48   | ...  | ...   |   |
| Virgo      | King                                | 0.61      | 14.89 | 4.77  | 5.24  | 4.33 <sup>†</sup>   | 5.26   | 0.17   | 0.13  |   |

High-energy cluster emission has been treated with either a two-dimensional Gaussian or King profile spatial model. Gaussian models are parameterized by the 68% surface intensity containment radius ( $R_{68}$ ) and King profiles are fitted to the X-ray surface intensity (see text).  $\langle \epsilon_{CR}/\epsilon_{Th} \rangle$  represents the volume-averaged CR-hadron-to-thermal energy density ratio assuming that hadronic CRs trace the ambient thermal gas distribution and are described by a power-law spectrum,  $N_p(E) \propto E^{-\alpha_p}$ . Upper limits to  $\langle \epsilon_{CR}/\epsilon_{Th} \rangle$  are computed using the most constraining energy bands (indicated by †). Notes from Table 2 also apply here.

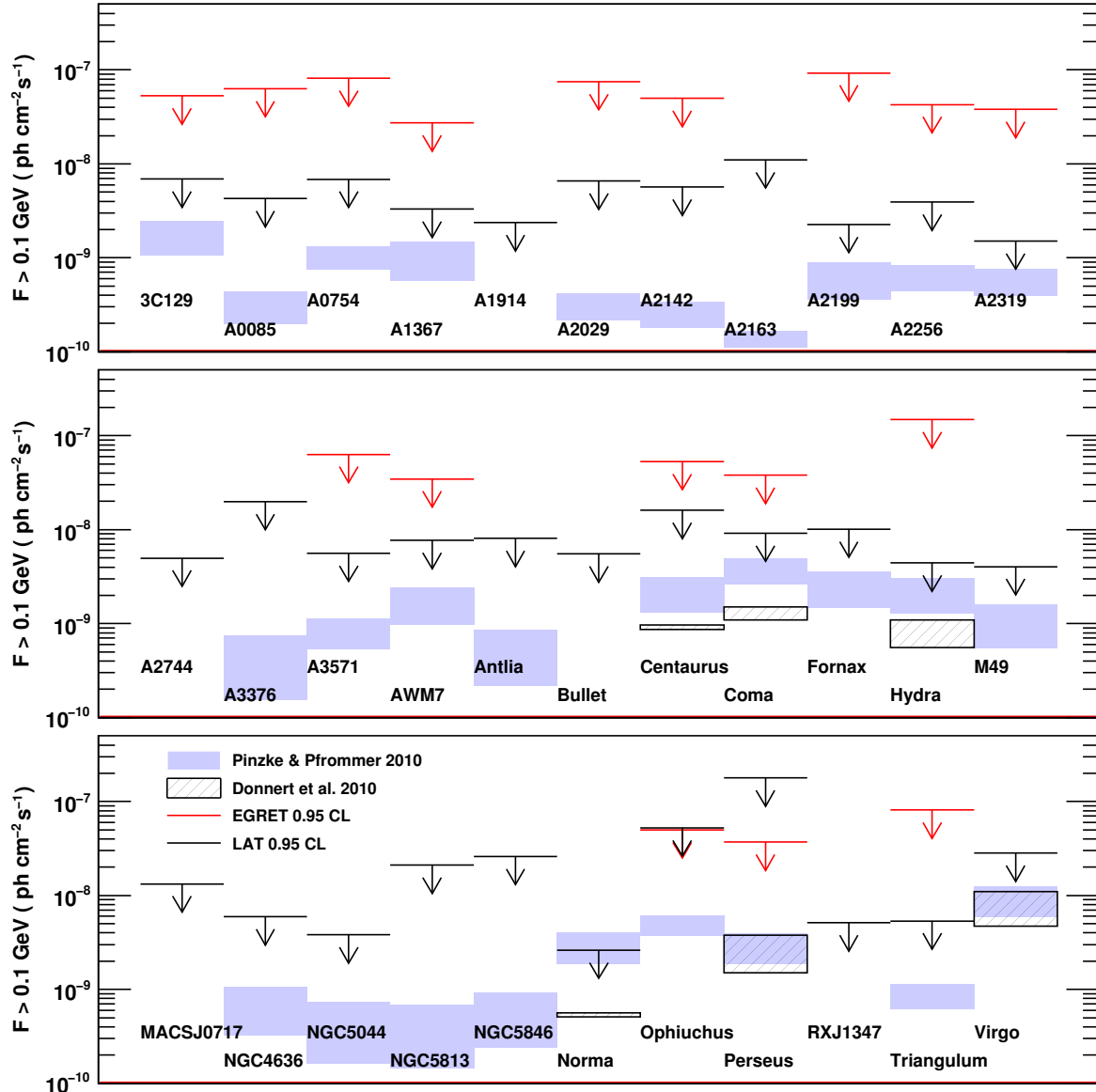


FIG. 1.— Photon flux upper limits derived from *Fermi*-LAT observations of galaxy clusters (assuming unresolved gamma-ray emission) are compared to EGRET results (Reimer et al. 2003) and to recent predictions based on the numerical simulations of Pinzke & Pfrommer (2010) (flux from within one virial radius) and Donnert et al. (2010). The LAT integral fluxes presented in Table 2 have been extrapolated to  $> 0.1 \text{ GeV}$  for ease of comparison.